Planet Space Sci., Vol. 34, No. 2, pp. 131-144, 1986
Printed in Great Britain.

0032-0633/86 $3.00 + 0.00

THE ROLE OF NITRIC OXIDE ON THE ZONALLY AVERAGED STRUCTURE OF THE THERMOSPHERE: SOLSTICE CONDITIONS FOR SOLAR CYCLE MINIMUM

J.-Cl. GÉRARD
Institut d'Astrophysique, Université de Liège—4200 Cointe-Liège, Belgium

and

R. G. ROBLE
High Altitude Observatory, National Center for Atmospheric Research*, P.O. Box 3000, Boulder, CO 80307, U.S.A.

(*Received* 1 *August* 1985)

Abstract—A zonally averaged chemical-dynamical model of the Earth's thermosphere is used to investigate the importance of nitric oxide 5.3-μm cooling in controlling the dynamic structure of the thermosphere. The model calculates the zonally averaged circulation, temperature, major atmospheric constituents, and the odd-nitrogen distributions self-consistently for solstice conditions during solar cycle minimum. The NO infrared cooling competes with downward molecular conduction in the upper thermosphere and reaches a maximum of ~ 500 K day^{-1} near 170 km at high summer latitudes. The primary effect of the 5.3-μm cooling is to weaken the summer-to-winter latitudinal temperature gradient, which in turn weakens the summer-to-winter meridional circulation. In the upper thermosphere NO 5.3-μm cooling reduces the summer-to-winter pole temperature difference by about 45 K with an 8 ms^{-1} reduction in the zonally averaged meridional wind velocity. There are corresponding reductions in the vertical and mean zonal wind velocities. The reduction of the mean circulation and latitudinal temperature gradient results in changes in composition of about -40% for O_2 and $+15\%$ for O in the upper thermosphere at high summer latitudes. The results suggest that NO 5.3-μm cooling has an important effect on the overall dynamic structure of the thermosphere, and it should be particularly important during solar maximum conditions and geomagnetic storms when the NO densities and neutral gas temperature increase substantially.

1. INTRODUCTION

The vertical thermal structure of the thermosphere is controlled primarily by a balance between the absorption of solar u.v. radiation by atmospheric constituents and downward molecular conduction. High-latitude heat sources caused by auroral particle precipitation and Joule dissipation of auroral currents also contribute to the heat budget of the thermosphere. Until recently, it was generally assumed that the heat absorbed in the thermosphere was conducted downward to the vicinity of the lower thermosphere and upper mesosphere where it was ultimately radiated to space by optically active minor atmosphere constituents, such as CO_2 and O_3. The only *in-situ* radiative cooling mechanism considered in the thermosphere was the 63-μm emission from the $O^3P_1 \rightarrow O^3P_2$ transition (Bates, 1951). A rocket measurement of the O(^{3}P) emission rate between 90 and 180 km by Grossman and Offermann (1978) showed that the 63-μm emission rate was considerably smaller than what would be expected from local thermodynamic equilibrium. This measurement suggests that the 63-μm line is not in local thermodynamic equilibrium. A further reduction of the intensity of the 63-μm emission is caused by the optical thickness of the O($^3P_1 - {}^3P_2$) transition below 150 km (Kockarts and Petermans, 1970). Consequently, O(^{3}P) emission is now considered an inefficient cooling process of the thermosphere. In the absence of an efficient heat loss in the lower thermosphere, current models lead to two difficulties:

- —the calculated temperature gradient is steeper than observed values near 120 km (Kockarts, 1975; Donahue and Carignan, 1975);
- —the calculated global mean exospheric temperature is larger than measured values, especially during solar maximum activity periods (Roble and Emery, 1983).

The potential role of the fundamental band of nitric oxide at 5.3-μm in the heat budget was suggested by

*The National Center for Atmospheric Research is sponsored by the National Science Foundation.

Gordiets and Markov (1977). This suggestion was stimulated by the satellite observations of substantial molecular emission in the 4.5–8.5-μm region by Markov *et al.* (1977).

Ogawa (1976) and Gordiets *et al.* (1978) calculated the 5.3-μm emission rate distribution from various sources, some of which do not contribute to remove heat from the ambient atmosphere. Enhancements of the 5.3-μm band during periods of strong magnetic activity were detected from the ground by Stair *et al.* (1975). Rawlins *et al.* (1981) and Reidy *et al.* (1982) measured emission rates in the 3–25 MR range at high latitudes. These emissions were associated with the increase in NO concentration generated by the interaction of auroral energetic particles with the atmosphere. Kockarts (1980) showed that the NO emission is never in local thermodynamic equilibrium (LTE) above 120 km and demonstrated that this process is important in the thermospheric energy budget, especially at locations with large NO densities. He gave an expression for the 5.3-μm cooling rate that depends on the local temperature and atmospheric densities. To reexamine the global average energy budget of the thermosphere, Roble and Emery (1983) solved the one-dimensional globally averaged heat conduction equation balancing radiative sources and sinks and downward conduction simultaneously with the hydrostatic equation. They used updated absorption cross-sections and u.v. solar fluxes based on *Atmosphere Explorer* measurements and concluded that the effect of the NO cooling on the global mean temperature is small during solar minimum activity periods but becomes important at solar cycle maximum, when both NO and temperature are larger. Gordiets *et al.* (1982) presented some numerical models of the thermospheric heat budget and concluded that radiational cooling by NO above 130 km and by CO_2 below 130 km dominate over eddy turbulent heat dissipation. Their model also showed a considerable reduction of the daily mean exospheric temperature when the NO cooling term was included.

So far, discussions and analysis of the role of the NO cooling have been based on one-dimensional descriptions of the problem. Besides, the NO vertical profiles adopted for these studies were somewhat arbitrary and not necessarily consistent with the adopted temperature and neutral density distribution. In this study, we use an updated version of the zonally averaged chemical-dynamical model described by Roble and Kasting (1984) (hereafter referred to as Paper I). The steady-state perturbation temperature, wind components, N_2, O_2 and O concentrations are calculated from pole to pole in the upper mesophere and thermosphere. The NO density is calculated using the two-dimensional odd-nitrogen model by Gérard *et al.* (1984) (Paper II). The two models are coupled in such a way as to obtain consistent values for the background atmosphere and for the odd-nitrogen concentrations. A solution without NO cooling is also compared with the complete solution to quantitatively assess the importance of the NO infrared emission on dynamics and composition. Finally, a diagnostic package is used to analyze the spatial distribution of the various terms of the thermodynamic equation and evaluate the relative importance of the NO cooling.

2. MODEL

The model used to calculate the zonally averaged circulation, temperature and compositional structure of the thermosphere in this study is based on that described previously in Paper I. The Roble–Kasting model itself was based on an earlier version, described by Kasting and Roble (1981), which had been modified to include high-latitude heat sources in addition to the differential solar heating. This zonally averaged chemical-dynamical model of the thermosphere extends from 70 to 356 km and from pole to pole with a latitudinal grid of 5° increments. This vertical grid uses a "pseudo log pressure" coordinate z defined as:

$$z = -\log (P_o(r)/P_{oo})$$

where r is the geocentric altitude, P_o is the pressure of an atmosphere in diffusive equilibrium with a globally averaged vertical temperature distribution $T_o(r)$, and P_{oo} is the pressure at 70 km. The model solves a system of equations that includes the zonal and meridional momentum and the thermodynamic, continuity, hydrostatic, and diffusion equations for mass mixing ratios of the major constituents. Consequently, the model calculates the time-dependent two-dimensional distributions of the major neutral constituents, O_2, N_2 and O; temperature; pressure; and mean zonal, meridional, and vertical winds. The set of coupled energy and momentum neutral gas equations and the list of chemical reactions affecting odd-oxygen were given by Kasting and Roble (1981). The major modification in the context of this study is the addition of a cooling term in the thermodynamic equation to represent the i.r. emission of nitric oxide in the 5.3-μm band. The formulation, given by Kockarts (1980), is adopted and the cooling rate per unit mass due to NO infrared emission is given by

$$Q_{NO} = \frac{h\nu}{\rho}[\mathrm{NO}]\, A_{10} \exp\left(-\frac{h\nu}{kT}\right) \frac{k_{10}[\mathrm{O}]}{k_{10}[\mathrm{O}] + A_{10}}, \quad (1)$$

with:

$h\nu$ ($=3.73\times10^{-13}$ erg) the energy of photons in the 5.3-μm band;
ρ the local mass density;
A_{10} ($=13.3\ s^{-1}$) the transition probability of the NO fundamental band;
k_{10} the vibrational relaxation coefficient of the process:

$$NO(v=1)+O \rightarrow NO(v=0)+O.$$

Atomic oxygen is considerably more effective than O_2 and N_2 in quenching vibrationally excited NO. We use the value $k_{10}=6.5\times10^{-11}\ cm^3s^{-1}$ obtained at 300 K by Fernando and Smith (1979). The temperature dependence of this coefficient has not been determined, and so has been neglected in these calculations. A temperature dependence for this coefficient may quantitatively affect the results described below. The last term of equation (1) represents the departure from LTE (LTE corresponds to a value of 1 for this term). Actually, in the Earth's thermosphere this term is everywhere less than 1 and the 5.3-μm emission is not in LTE.

The nitric oxide concentration used in (1) is obtained from the 2-dimensional zonally averaged model of odd nitrogen described in Paper II. However, in order to calculate NO densities consistent with the major constituent concentrations and with the wind and temperature fields, the odd nitrogen model is coupled to the chemical-dynamical model. The NO distribution is recalculated at every time step by updating the production and loss terms and the vertical and meridional wind components w and v in the continuity equation, which controls the NO and N(^{4}S) concentrations:

$$\frac{\partial n_i}{\partial t}=P_i-l_in_i-\frac{\partial\phi_i}{\partial r}-\left[\frac{1}{r^2}\frac{\partial(r^2w)}{\partial r}-\frac{1}{r\sin\theta}\frac{\partial(v\sin\theta)}{\partial\theta}\right]n_i \quad (2)$$

where P_i and l_i are the chemical production and loss rates of n_i respectively, r and θ the geocentric altitude and colatitude, and ϕ_i the vertical molecular and eddy diffusion flux.

A 5-min time step is used to calculate the velocity and perturbation temperature fields. The chemical calculation is alternated with the dynamical calculation every 0.2 days to solve the continuity equations for the major constituents. The odd nitrogen is also updated every 0.2 days, and the new NO concentration is used to recalculate the net heating term of the thermodynamic equation at the following iteration. The boundary conditions are identical to those used in Papers I and II. In particular, the latitudinal profile of the meridional wind at the lower boundary condition is adopted from the model of Garcia and Solomon (1983). The initial major constituents, temperature, and wind fields are the solutions obtained in Paper I for conditions of moderate magnetic activity.

The odd-nitrogen concentrations calculated in Paper II for the "solar only" model with winds are used as initial values for the odd-nitrogen calculation. The combined system is integrated until it converges. Although the chemical-dynamical and odd-nitrogen models used for these calculations are similar to those described in Papers I and II, respectively, some changes have been made to update the photochemistry and ionization rates; these changes are described below.

The O_2 photolysis is produced by direct absorption of photons in the Schumann–Runge bands and continuum, and the Lyman-alpha line, and by indirect dissociation due to absorption of e.u.v. radiation. The dissociation rate in the Schumann–Runge continuum is now based on the parameterization given by Torr *et al.* (1980) which divides the 1375–1750 Å range into eight wavelength intervals. However, their values were based on the solar irradiance measurements by Heroux and Higgins (1977), which are globally 34% less than the high-resolution measurements by Rottman (1981). Consequently, the photodissociation rates have been recalculated for each interval by using the irradiance values listed by Rottman for 1972–1977 minimum solar activity conditions. The photoionization rates are calculated using the effective absorption and ionization cross-sections derived by Torr *et al.* (1979) for 37 intervals between 50 and 1050 Å. We have adopted the solar e.u.v. fluxes measured with the *Atmosphere Explorer* spectrometers during the minimum of the previous solar cycle. As previously, the e.u.v. O_2 dissociation rate is obtained by assuming that one O_2 molecule is dissociated for each absorption of an e.u.v. photon.

The latitudinal distribution of both the ionization by energetic particles and particle heating at high latitudes was previously modeled by a Gaussian function centered at 70° to represent the latitudinal distribution and a Chapman function for the altitude dependence. In the present model, the latitudinal distribution of the total particle energy flux is derived from the statistical analysis of the *Atmosphere Explorer* particle measurements by Spiro *et al.* (1982). Their table of auroral electron energy fluxes for values of the AE index < 300 nT was averaged over local time in order to obtain the mean latititudinal energy flux distribution $F_E(\theta)$. The vertical distribution of the ionization rate

is given by:

$$P(z, \theta) = AP_o(\theta) \exp [1-x-e^{-x}], \quad (3)$$

with

$$x = \frac{Z_a - Z}{D_H}$$

where D_H represents the topside scale height and Z_a the altitude of the peak ionization rate. This altitude is obtained by computing for each latitude bin the penetration depth of the electrons with initial energy E_o using the energy-range relationship given by Lazarev (1967).

The latitudinal distribution of the characteristic energy is again obtained by zonally averaging the observational results of Spiro *et al.* (1982) for low magnetic activity conditions.

The value of the constant A in (3) is obtained by normalizing the spheric integral of $P(z, \theta)$ to the total particle energy input. This energy input is calculated by partitioning the total planetary energy input into particle, Joule, and conduction heating in a way similar to Paper I. For example, it is assumed that Joule heating is 2.5 times stronger in the summer than in the winter hemisphere (Dickinson *et al.*, 1977; Roble *et al.*, 1977), but particle heating is equal in both hemispheres. The total global energy heating of magnetospheric origin is 5×10^{10} W, as assumed in Paper I to model magnetically quiet periods.

3. RESULTS

3a. *Dynamics*

The calculated circulation and temperature are illustrated in Fig. 1 for the case when the NO cooling term is included in the thermodynamic equation. They correspond to the same geophysical conditions as Fig. 4 of Paper I except for the presence of the 5.3-μm emission term in the thermodynamic equation. The summer-to-winter meridional wind (v) reaches peak values of about 30 ms^{-1} near 60° in the summer hemisphere (Fig. 1a). This maximum is associated with the location of the auroral Joule heating source, which reinforces the solar-driven meridional circulation. In the winter hemisphere, a high-latitude reverse cell opposes the mean summer-to-winter circulation as a consequence of the high-latitude heating. This pattern is very similar to that obtained by Roble and Kasting (1984) although the maximum velocity has decreased from over 35 ms^{-1} to about 30 ms^{-1}. The size of the winter polar reverse cell is also smaller than before.

The zonal wind (u) field shown in Fig. 1b is directed eastward in the winter and westward in the summer hemisphere. The zonal jets peak near the lower boundary as a consequence of the boundary prescriptions as discussed in Paper I. The zonal velocities decrease at higher altitude as a result of the F-region ion drag. A secondary maximum is localized near 65° in summer and is associated with the Coriolis torque acting on the peak of the meridional wind. The reversal of the zonal wind direction above 60° and 240 km is caused by the equatorward flow generated by the high-latitude Joule heating. This pattern is again qualitatively similar to the results of Paper I, but the extent of the westward cell in winter and the magnitude of the wind have decreased.

The calculated distribution of temperature perturbation ΔT from the global mean is illustrated in Fig. 1c. The perturbation temperature reaches about 130 K near the summer pole at high altitudes and decreases to -30 K near 50° in summer. Near the winter pole ΔT rises to about -10 K as a result of the high-latitude heating. This structure is caused by the high-latitude heat source which moves the temperature minimum away from the pole. Near 110 km, the latitudinal temperature gradient is reversed, with values of ΔT about 50 K at high winter latitudes and about -10 K at the summer pole. Comparison with Fig. 4c of Paper I shows that the latitudinal gradient of temperature at high altitudes is reduced from about 190 to 150 K. As will be discussed below, this is a direct consequence of the inclusion of the NO cooling term in the thermodynamic equation. Adiabatic heating and cooling are largely responsible for the reversal of the temperature gradient in the lower thermosphere, as will be discussed in a later section.

The calculated vertical wind (w) shown in Fig. 1d is upward in the poleward section of the summer hemisphere as an effect of the thermal expansion due to the solar and high-latitude heating. The maximum velocity of about 100 cm s^{-1} is reached over the summer pole. A downward motion is obtained in most of the winter hemisphere, but a rising motion is generated by the high-latitude heat source near the winter pole. The general pattern is similar to Fig. 4 of Paper I with a reduction of the maximum upward wind in summer and near the winter pole.

3b. *Composition*

The O_2, O and N_2 zonal mean concentrations associated with the circulation pattern are shown in Fig. 2. It shows the same global structure as Fig. 5 of Paper I, although the absolute densities are somewhat different. Two peaks of atomic oxygen reaching $\sim 3 \times 10^{11}$ cm^{-3} are obtained in the lower thermosphere near 60° in winter and near the summer pole. The equatorial trough in O results from the maximum of the

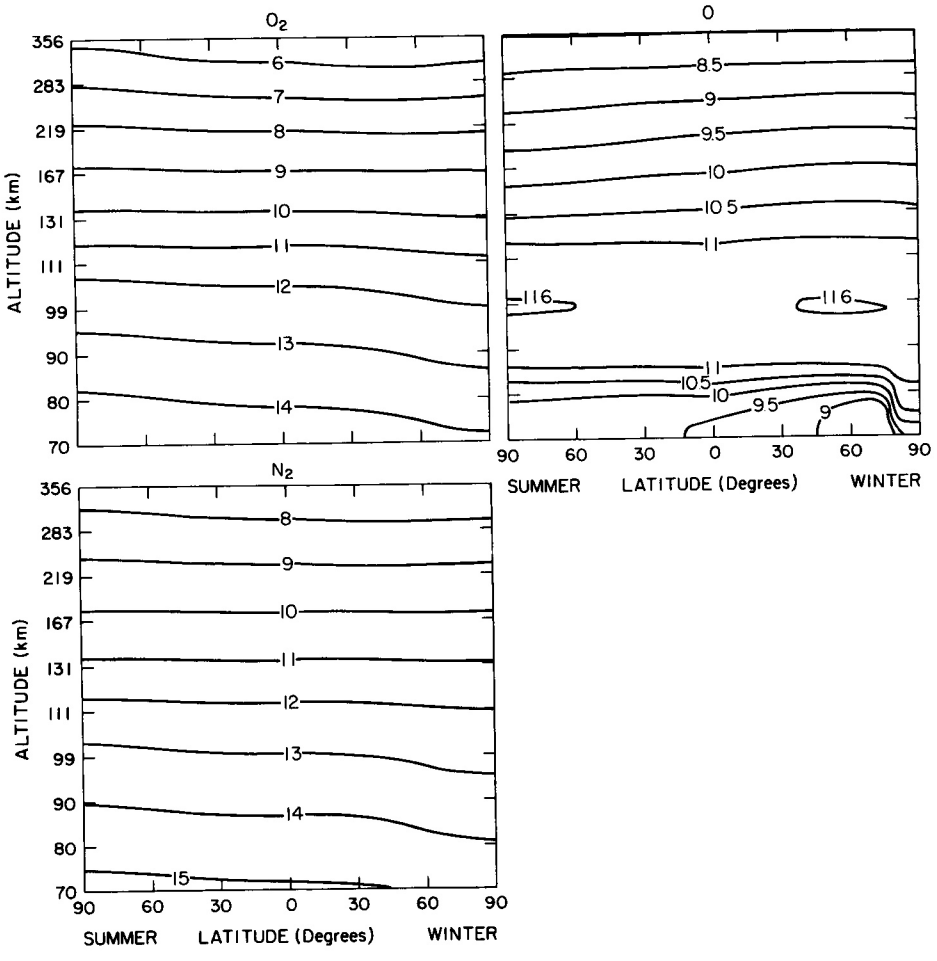

FIG. 2. CONTOURS OF CALCULATED ZONALLY AVERAGED DISTRIBUTION OF THE MAJOR THERMOSPHERIC CONSTITUENTS WITH NO COOLING FOR SOLSTICE CONDITIONS DURING SOLAR CYCLE MINIMUM. (a) $\log_{10} O_2$ (cm^{-3}); (b) $\log_{10} O$ (cm^{-3}); (c) $\log_{10} N_2$ (cm^{-3}).

winter hemisphere, the vertical distribution curve becomes very flat and, at latitudes above 70°, the NO density decreases monotonically with altitude from the mesosphere to the upper thermosphere. This shape is due to the absence of solar radiation and thus of NO photolysis in this region. As a consequence, the nitric oxide produced in the thermosphere by ion-molecule reactions and particle-induced dissociation is carried downward by turbulent transport. These characteristics of the NO two-dimensional distribution are also in agreement with the results by Solomon *et al* (1982). In the *F*-region, the NO summer densities exceed the winter values by a factor of 4.

This difference is explained by the asymmetry in the temperature field and the O_2 compositional distribution. At high altitudes, the major source of NO is the reaction between O_2 and ground state $N(^4S)$ atoms:

$$N(^4S) + O_2 \rightarrow NO + O,$$

whose rate coefficient is strongly temperature dependent. Consequently, the production rate and the concentration of NO is substantially larger near the summer pole, which is about 130 K warmer than the winter pole. In comparison with the results of Paper II, the lower peak NO concentration near 70° in summer and the absence of a peak in the winter auroral zone are due primarily to the different latitude and altitude distribution of the ionization source and to a minor extent to the slightly different neutral composition.

The NO meridional distribution calculated in Paper

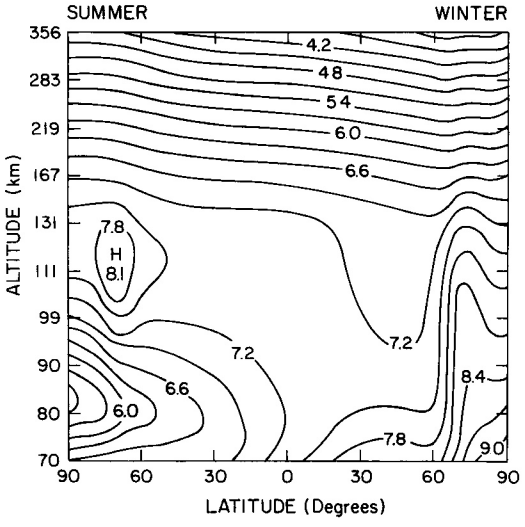

FIG. 3. CONTOURS OF LOG_{10} OF ZONALLY AVERAGED NITRIC OXIDE CONCENTRATION (cm^{-3}) CALCULATED FOR SOLSTICE QUIET CONDITIONS AND SOLAR CYCLE MINIMUM.

II was shown to be in good agreement with the available satellite measurements of the latitudinal distribution during solar minimum cycle conditions at solstice (Cravens *et al.*, 1986). Since the shape of the distribution and the absolute concentrations are not considerably different from the results of Paper II, the values in Fig. 3 may also be considered as a valid respresentation of the nitric oxide distribution for periods of low geomagnetic activity.

3c. *Effect of the* 5.3 μm *cooling*

In order to make a detailed evaluation of the role of the 5.3-μm cooling, the two-dimensional calculations were repeated with the Q_{NO} term set to zero in the thermodynamic equation. The initial wind, temperature, background composition, and NO density fields were identical, and the two calculations were made over the same model time. In this way, any difference between the two sets of results reflects the effect of the NO 5.3-μm band.

Figure 4 illustrates the differences on the dynamic fields u, v, ΔT, and w obtained by subtracting the solution for the $Q_{NO} = 0$ case from the solutions shown in Fig. 1.

The calculated difference in temperature shown in Fig. 4c results from the combination of the direct effect of Q_{NO} on the net heating rate Q' and the indirect consequences of perturbations in the wind and composition fields. The importance of the various terms will be described quantitatively below. The most conspicuous effect of nitric oxide in Fig. 4c is to decrease the temperature in the summer hemisphere and increase it in the winter hemisphere. The maximum difference is nearly −30 K at 180 km at the summer pole and 22 K near the upper boundary at the winter pole. Since the calculated summer thermosphere is about 120 K warmer than the winter hemisphere, the effect of the 5.3-μm emission is to decrease the temperature contrast between the two hemispheres by about 40 K. This difference is explained by the larger NO concentrations and perturbation temperatures obtained in the summer hemisphere (Fig. 3), which tend to cool the summer hemisphere more efficiently. Another region of temperature decrease is observed near 120 km at high winter latitudes and is associated with the large NO concentrations in the dark polar lower thermosphere. The globally averaged temperature $T_o(z)$ used in this model is identical to that used by Kasting and Roble (1981). It corresponds to an exospheric temperature of 820 K and was obtained from the MSIS model atmosphere for solar minimum conditions above 120 km (F 10.7 cm = 80, Ap = 4) smoothly connected to the 1976 *U.S. Standard Atmosphere* below. Since the diabatic heating term in the second member of the energy equation represents the perturbation heating with respect to the mean value, only temperature perturbations from the global average may be obtained with this model. Consequently, this approach does not provide any estimate of the decrease in the global temperature due to the NO cooling, but it yields the thermal differences from a prescribed global average value.

The differences in the wind components are shown in Fig. 4a, b, and d in $cm\,s^{-1}$. The high-altitude meridional wind velocity (Fig. 4a) is decreased by up to 8.5 $m\,s^{-1}$ by the NO cooling. This weakening of the summer-to-winter meridional wind is a consequence of the lower latitudinal temperature gradient shown in Fig. 4c. The zonal wind pattern is mostly affected in the upper thermosphere. The lower altitude zonal wind is controlled primarily by the value of the meridional wind at the lower boundary which is identical for both cases. The westward flow in the summer hemisphere and the eastward flow in winter are both weakened by the presence of the 5.3-μm cooling, with the exception of the intensification of the eastward flow at high winter latitudes. An increase of the zonal circulation is also produced near 125 km at summer mid-latitudes. The vertical wind circulation (Fig. 4d) is also weakened by the NO cooling. The upwelling and downwelling, in the summer and winter hemisphere respectively, are decreased by about 20%. The general conclusion is that the major effect of the 5.3-μm NO cooling is to weaken the circulation driven by the solar and magnetospheric

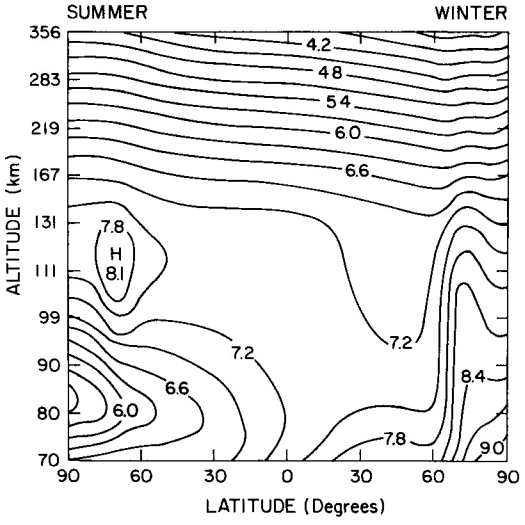

FIG. 3. CONTOURS OF LOG_{10} OF ZONALLY AVERAGED NITRIC OXIDE CONCENTRATION (cm^{-3}) CALCULATED FOR SOLSTICE QUIET CONDITIONS AND SOLAR CYCLE MINIMUM.

II was shown to be in good agreement with the available satellite measurements of the latitudinal distribution during solar minimum cycle conditions at solstice (Cravens *et al.*, 1986). Since the shape of the distribution and the absolute concentrations are not considerably different from the results of Paper II, the values in Fig. 3 may also be considered as a valid respresentation of the nitric oxide distribution for periods of low geomagnetic activity.

3c. *Effect of the* 5.3 μm *cooling*

In order to make a detailed evaluation of the role of the 5.3-μm cooling, the two-dimensional calculations were repeated with the Q_{NO} term set to zero in the thermodynamic equation. The initial wind, temperature, background composition, and NO density fields were identical, and the two calculations were made over the same model time. In this way, any difference between the two sets of results reflects the effect of the NO 5.3-μm band.

Figure 4 illustrates the differences on the dynamic fields u, v, ΔT, and w obtained by subtracting the solution for the $Q_{NO} = 0$ case from the solutions shown in Fig. 1.

The calculated difference in temperature shown in Fig. 4c results from the combination of the direct effect of Q_{NO} on the net heating rate Q' and the indirect consequences of perturbations in the wind and composition fields. The importance of the various terms will be described quantitatively below. The most conspicuous effect of nitric oxide in Fig. 4c is to decrease the temperature in the summer hemisphere and increase it in the winter hemisphere. The maximum difference is nearly -30 K at 180 km at the summer pole and 22 K near the upper boundary at the winter pole. Since the calculated summer thermosphere is about 120 K warmer than the winter hemisphere, the effect of the 5.3-μm emission is to decrease the temperature contrast between the two hemispheres by about 40 K. This difference is explained by the larger NO concentrations and perturbation temperatures obtained in the summer hemisphere (Fig. 3), which tend to cool the summer hemisphere more efficiently. Another region of temperature decrease is observed near 120 km at high winter latitudes and is associated with the large NO concentrations in the dark polar lower thermosphere. The globally averaged temperature $T_o(z)$ used in this model is identical to that used by Kasting and Roble (1981). It corresponds to an exospheric temperature of 820 K and was obtained from the MSIS model atmosphere for solar minimum conditions above 120 km (F 10.7 cm = 80, Ap = 4) smoothly connected to the 1976 *U.S. Standard Atmosphere* below. Since the diabatic heating term in the second member of the energy equation represents the perturbation heating with respect to the mean value, only temperature perturbations from the global average may be obtained with this model. Consequently, this approach does not provide any estimate of the decrease in the global temperature due to the NO cooling, but it yields the thermal differences from a prescribed global average value.

The differences in the wind components are shown in Fig. 4a, b, and d in cm s^{-1}. The high-altitude meridional wind velocity (Fig. 4a) is decreased by up to 8.5 m s^{-1} by the NO cooling. This weakening of the summer-to-winter meridional wind is a consequence of the lower latitudinal temperature gradient shown in Fig. 4c. The zonal wind pattern is mostly affected in the upper thermosphere. The lower altitude zonal wind is controlled primarily by the value of the meridional wind at the lower boundary which is identical for both cases. The westward flow in the summer hemisphere and the eastward flow in winter are both weakened by the presence of the 5.3-μm cooling, with the exception of the intensification of the eastward flow at high winter latitudes. An increase of the zonal circulation is also produced near 125 km at summer mid-latitudes. The vertical wind circulation (Fig. 4d) is also weakened by the NO cooling. The upwelling and downwelling, in the summer and winter hemisphere respectively, are decreased by about 20%. The general conclusion is that the major effect of the 5.3-μm NO cooling is to weaken the circulation driven by the solar and magnetospheric

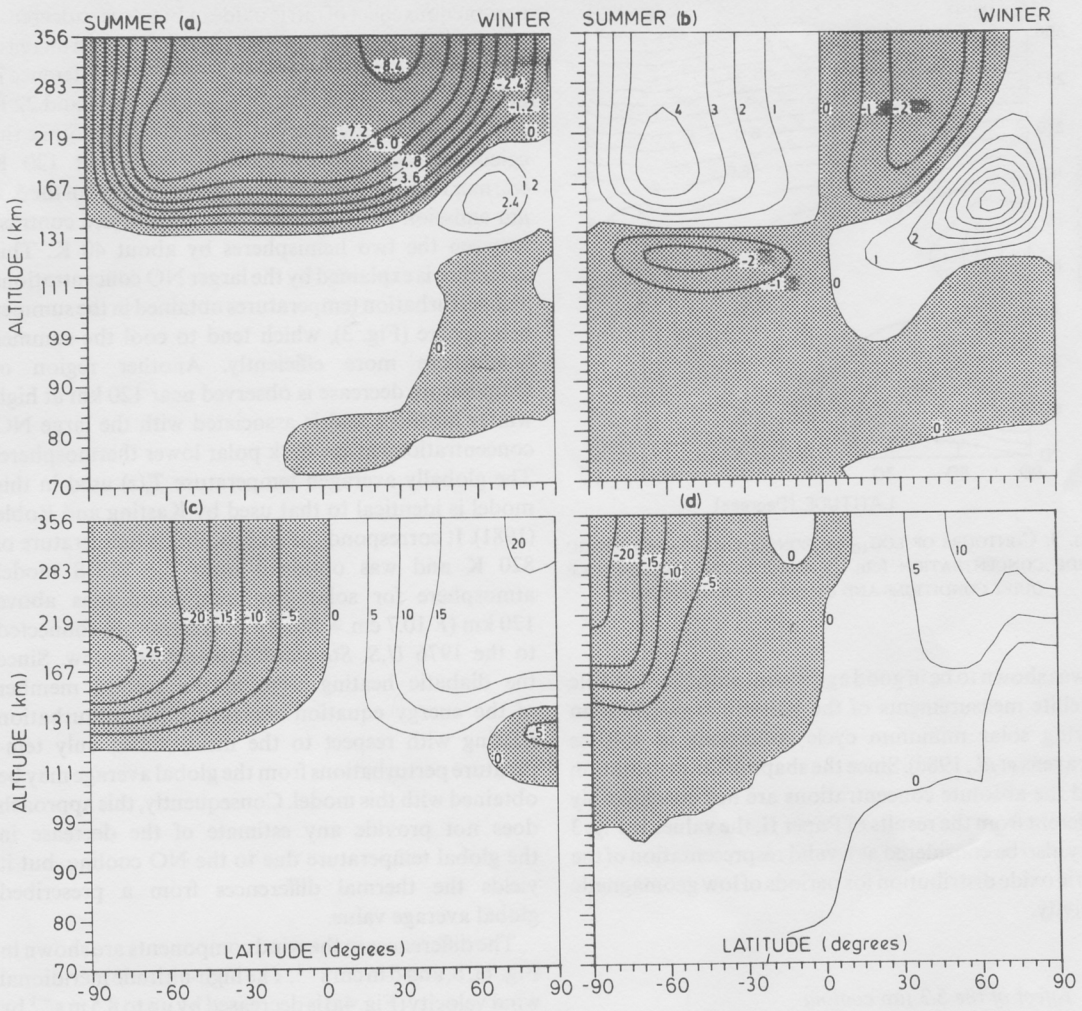

FIG. 4. CONTOURS OF DIFFERENCES BETWEEN CALCULATED CIRCULATION AND TEMPERATURE FIELDS WITH AND WITHOUT 5.3-μm NO COOLING.
(a) Meridional wind (m s^{-1}); (b) zonal wind (m s^{-1}); (c) perturbation temperature (K); (d) vertical wind (cm s^{-1}). Sign conventions are identical to those used in Fig. 1.

heating sources. This cooling term Q_{NO} has a two-fold dependence on temperature. It depends directly on T by the exponential term in equation (1) and indirectly through the NO density, which, in the upper thermosphere, also increases with temperature. Consequently, this cooling term maximizes in the warmest regions of the thermosphere, tending to decrease the latitudinal temperature gradients and slow down the circulation. The effects on dynamics also generate changes in composition. Figure 5 shows the fractional change of the O_2, N_2 and O densities produced by the Q_{NO} term. Both O_2 and N_2 densities increase in the winter hemisphere and decrease in summer. The magnitude of the relative perturbation, however, is different. It reaches over 20% of the O_2 and 5% of the N_2 densities at 200 km. These changes are a consequence of the perturbation of the temperature distribution and scale heights and of the vertical wind velocity. The atomic oxygen density varies by up to 15%. An increase of O is calculated over most of the thermosphere with the exception of a latitudinal zone centered on 50° latitude in the winter hemisphere. This complex behaviour is partly explained by the weakening of the summer-to-winter circulation, which transports the atomic oxygen produced in the summer hemisphere into the winter regions. Another factor is

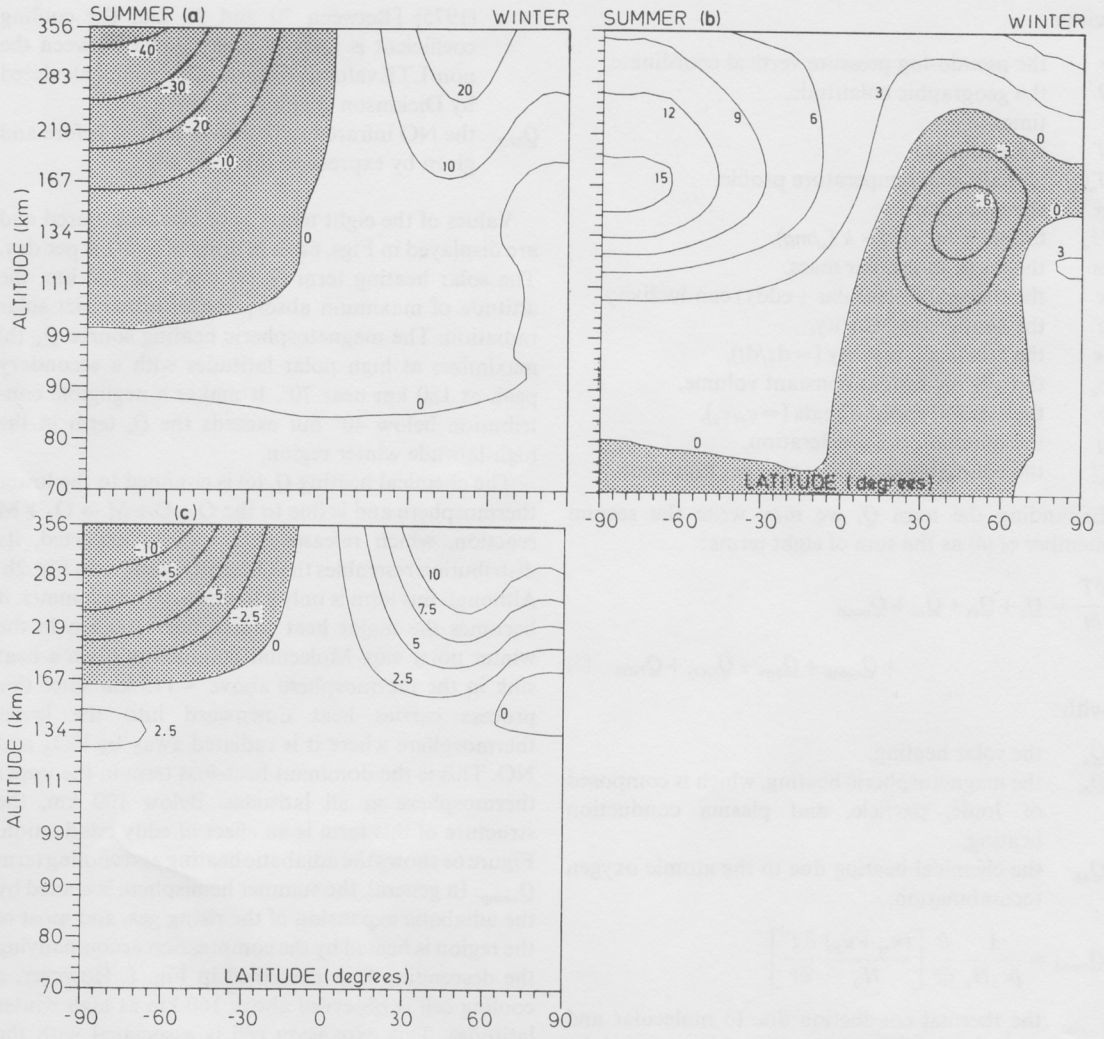

FIG. 5. CONTOURS OF RELATIVE DIFFERENCES IN PERCENT BETWEEN CALCULATED COMPOSITION FIELDS WITH AND WITHOUT 5.3 μm NO COOLING.
(a) $\Delta O_2/O_2$; (b) $\Delta O/O$; (c) $\Delta N_2/N_2$.

the decrease in vertical velocity, which causes less upwelling of O_2 and N_2 in the auroral regions.

4. THE THERMODYNAMIC EQUATION

The primary effect of the NO cooling in the thermosphere is to perturb the thermospheric temperature distribution as illustrated in Fig. 4c. These changes in the temperature distribution modify in turn the global-scale transport, which subsequently perturbs the chemical composition. The role of the 5.3-μm NO radiation can be evaluated by comparing its values with the other terms of the energy equation. For this purpose, a diagnostic package has been developed to evaluate the different terms of the thermodynamic equation from the final solution.

The zonally averaged thermodynamic equation may be written:

$$\frac{\partial T}{\partial t} = \frac{1}{\rho H_o c_v}\left(\frac{\kappa}{H_o}\frac{\partial T}{\partial z}\right) - \frac{v}{r}\left(\frac{\partial T}{\partial \theta} - \frac{kT}{mc_v}\frac{\partial \ln \rho}{\partial \theta}\right) + \frac{Q}{c_v} - w\left(\frac{\gamma}{H_o}\frac{\partial T}{\partial z}\frac{g}{c_v}\right), \quad (4)$$

with:

z the pseudo-log pressure vertical coordinate,
θ the geographic colatitude,
t time,
T temperature,
$T_o(z)$ global mean temperature profile,
ρ the mass density,
H_o the scale factor ($= kT_o/mg$),
m the mean molecular mass,
κ the thermal (molecular + eddy) conductivity,
v the southward velocity,
w the "vertical" velocity ($= \mathrm{d}z/\mathrm{d}t$),
c_v the specific heat at constant volume,
γ the ratio of specific heats ($= c_p/c_v$),
g the gravitational acceleration,
Q the net diabatic heating rate per unit mass.

Expanding the term Q, we may write the second member of (4) as the sum of eight terms:

$$\frac{\partial T}{\partial t} = Q_s + Q_m + Q_{ch} + Q_{\mathrm{cond}} + Q_{\mathrm{comp}} + Q_{\mathrm{adv}} + Q_{\mathrm{CO_2}} + Q_{\mathrm{NO}}, \quad (5)$$

with:

Q_s the solar heating,
Q_m the magnetospheric heating, which is composed of Joule, particle, and plasma conduction heating,
Q_{ch} the chemical heating due to the atomic oxygen recombination,

$$Q_{\mathrm{cond}} = \frac{1}{\rho c_v H_o} \frac{\partial}{\partial z}\left[\frac{(\kappa_m + \kappa_E)}{H_o}\frac{\partial T}{\partial t}\right],$$

the thermal conduction due to molecular and eddy heat conductivity. The eddy conductivity $\kappa_E = 2.5\ c_v\ \mu_E$ and the eddy viscosity μ_E parameterize the vertical transport of heat by turbulent transport which dominates over molecular conductivity κ_M below the turbopause,

$$Q_{\mathrm{comp}} = \frac{kT}{mc_v}\left(\frac{v}{r}\frac{\partial \ln \rho}{\partial \theta} + \frac{w}{H_o}\frac{\partial \ln \rho}{\partial z}\right),$$

the compressional adiabatic heating,

$$Q_{\mathrm{adv}} = -\frac{v}{r}\frac{\partial T}{\partial \theta} - \frac{w}{H_o}\frac{\partial T}{\partial z},$$

the ($-$v. grad T) temperature advection,
$Q_{\mathrm{CO_2}}$ the infrared radiative cooling by CO_2. Above 90 km, this term is calculated by using a Newtonian cooling coefficient based on the complete non-LTE approximation given by Dickinson *et al.* (1975) [Between 70 and 90 km, the cooling coefficient is linearly interpolated between the non-LTE value at 90 km and the value calculated by Dickinson (1973) at 70 km],
Q_{NO} the NO infrared radiation described before and given by expression (1).

Values of the eight terms have been contoured and are displayed in Figs. 6a–h in units of Kelvins per day. The solar heating term Q_s (a) peaks at 220 km, the altitude of maximum absorption of ultraviolet solar radiation. The magnetospheric heating source Q_m (b) maximizes at high polar latitudes with a secondary peak at 180 km near 70°. It makes a negligible contribution below 40° but exceeds the Q_s term in the high-latitude winter region.

The chemical heating Q_c (c) is confined to the lower thermosphere and is due to the $O + O + M \rightarrow O_2 + M$ reaction, which releases 5.11 eV. As expected, its distribution resembles the O density contour in Fig. 2b. Although this term is only a fraction of Q_s in summer, it becomes the major heat source near 100 km in the winter polar cap. Molecular conduction (d) is a heat sink in the thermosphere above ~115 km since this process carries heat downward into the lower thermosphere where it is radiated away by CO_2 and NO. This is the dominant heat-loss term in the upper thermosphere at all latitudes. Below 100 km, the structure of this term is an effect of eddy conduction. Figure 6e shows the adiabatic heating and cooling term Q_{comp}. In general, the summer hemisphere is cooled by the adiabatic expansion of the rising gas, and most of the region is heated by the compression accompanying the descending flow described in Fig. 1. However, a cooling cell is observed above 160 km at high winter latitudes. This expansion cell is associated with the upwelling generated by the heat source shown in Fig. 6d. The heat advection term Q_{adv} is shown in Fig. 6f. This term may be a source or a sink of heat, depending on the sign of the v. grad T term. It maximizes as a sink near 160 km in the summer hemisphere, where heat is transported away by the vertical and meridional wind. The same occurs at winter high latitudes, where the heat of magnetospheric origin is convected away by the high-latitude reverse cell.

The CO_2 radiation cooling term is contoured in Figure 6g. It becomes important below 110 km and increases toward lower altitudes. Its value decreases from the summer to the winter pole as a result of the latitudinal temperature gradient. Finally, contours of the NO 5.3-μm radiative term are shown in Fig. 6h. This term peaks nears 170 km in summer and 145 km in winter, the largest value (600 K day^{-1}) being reached at the summer pole. At all latitudes, Q_{NO}

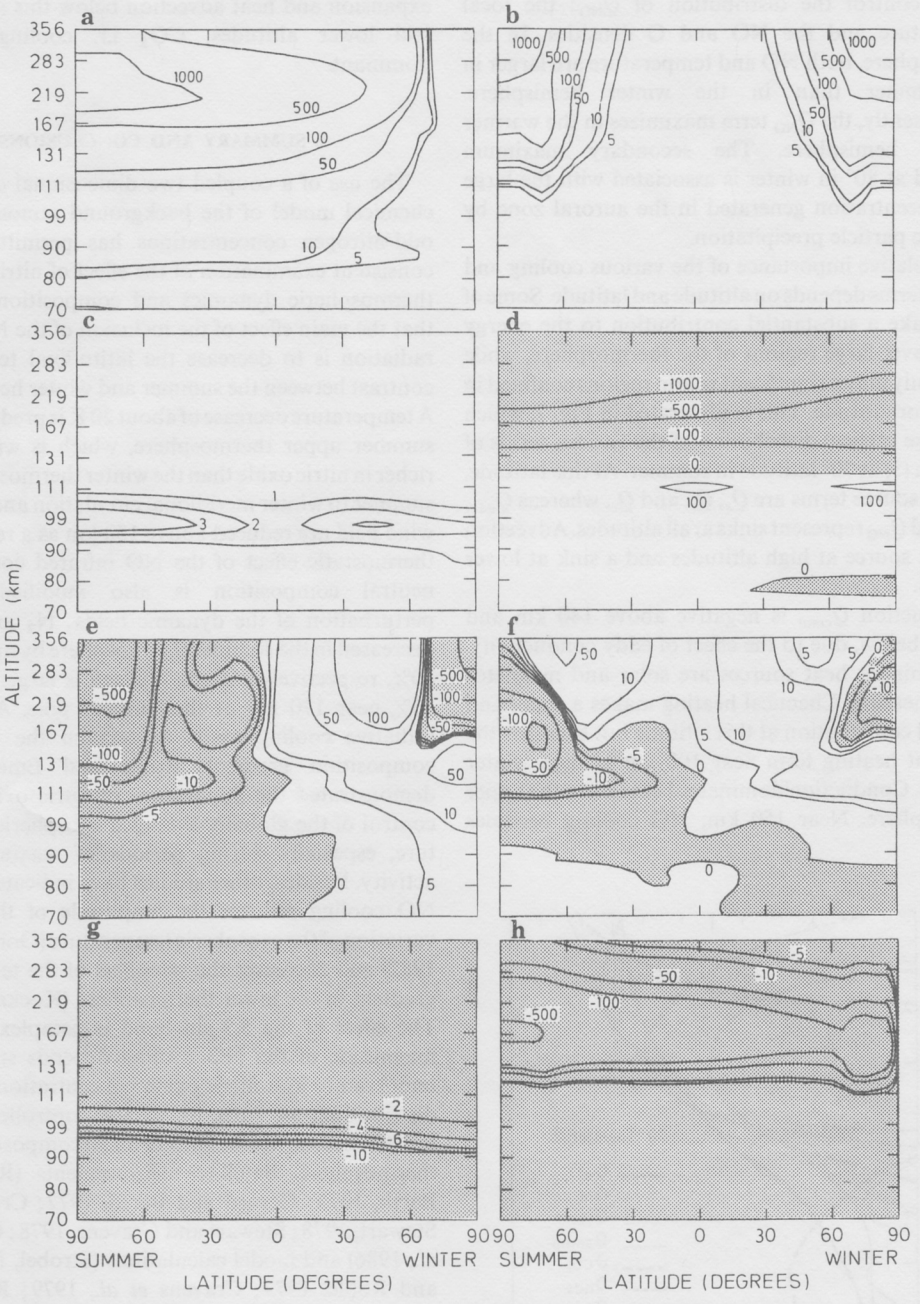

FIG. 6. CONTOURS OF THE VARIOUS HEATING AND COOLING TERMS OF THE THERMODYNAMIC EQUATIONS IN K day^{-1}.

(a) Solar u.v. and e.u.v. heating; (b) magnetospheric heating; (c) chemical heating; (d) transport by conduction; (e) adiabatic heating or cooling; (f) heat advection; (g) CO_2 cooling; (h) NO cooling. The shaded areas indicate regions of cooling.

decreases from the summer to the winter pole. Three factors control the distribution of Q_{NO}: the local temperature and the NO and O densities. In the thermosphere, both NO and temperature are larger in the summer than in the winter hemisphere. Consequently, the Q_{NO} term maximizes in the warmer summer hemisphere. The secondary maximum obtained at 80° in winter is associated with the large NO concentration generated in the auroral zone by energetic particle precipitation.

The relative importance of the various cooling and heating terms depends on altitude and latitude. Some of them make a substantial contribution to the energy budget over large regions of the thermosphere, while others only play a significant role in regions confined in latitude or altitude. This is illustrated in Fig. 7, which shows the vertical distribution of the various terms of equation (3) at 70° latitude in summer. At this latitude, the heat source terms are Q_s, Q_m and Q_c, whereas Q_{adv}, Q_{CO_2}, and Q_{NO} represent sinks at all altitudes. Advection is a heat source at high altitudes and a sink at lower altitudes.

Conduction Q_{cond} is negative above 140 km and positive below, due to the effect of eddy conductivity. The dominant heat sources are solar and magnetospheric heating. Chemical heating makes a small and localized contribution at this latitude but becomes the dominant heating term near 100 km at high winter latitudes. Conduction dominates heat loss in the upper thermosphere. Near 150 km, NO cooling becomes more important and competes with adiabatic expansion and heat advection below this altitude. At still lower altitudes, CO_2 i.r. cooling becomes dominant.

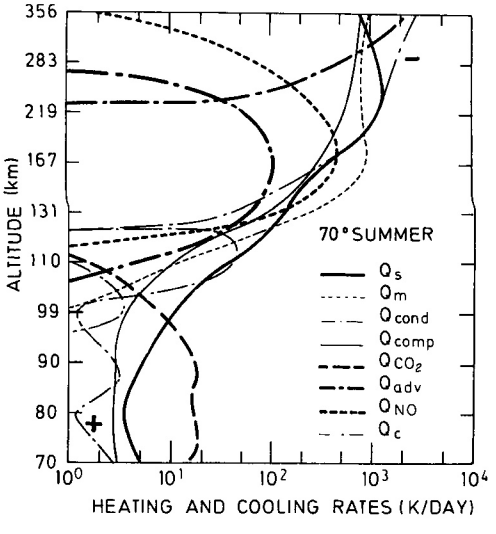

FIG. 7. VERTICAL DISTRIBUTION OF THE ABSOLUTE VALUE OF THE HEATING AND COOLING TERMS IN K day^{-1} AT 70° IN THE SUMMER HEMISPHERE.
The minus sign indicates negative (cooling) terms.

5. SUMMARY AND CONCLUSIONS

The use of a coupled two-dimensional dynamical-chemical model of the background atmosphere and odd-nitrogen concentrations has permitted a self-consistent examination of the effect of nitric oxide on thermospheric dynamics and composition. We find that the main effect of the inclusion of the NO 5.3-μm radiation is to decrease the latitudinal temperature contrast between the summer and winter hemispheres. A temperature decrease of about 20 K is predicted in the summer upper thermosphere, which is warmer and richer in nitric oxide than the winter thermosphere. The summer to winter meridional circulation and the zonal wind field are reduced above 130 km as a result of the thermostatic effect of the NO infrared cooling. The neutral composition is also modified by the perturbation of the dynamic fields: N_2 and O_2 are decreased in the summer thermosphere by up to 10 and 40%, respectively. Atomic oxygen is larger by about 15% near 170 km at the summer pole. Again, NO radiative cooling tends to weaken the latitudinal composition gradient. Roble and Emery (1983) demonstrated the importance of nitric oxide on the control of the globally averaged exospheric temperature, especially during periods of maximum solar activity. Besides, other studies have indicated that the NO cooling reduces the amplitude of the diurnal variation of the exospheric temperature (Gordiets *et al.*, 1982) and decreases the steepness of the temperature gradient in the lower thermosphere (Kockarts, 1980). The effect of the 5.3-μm band is complex since the magnitude of the NO cooling depends strongly on temperature and nitric oxide concentration. The NO distribution, in turn, is partly controlled by the temperature structure and chemical composition of the thermosphere. Satellite measurements (Rusch and Barth, 1975; Gérard and Barth, 1977; Cravens and Stewart, 1978; Stewart and Cravens, 1978; Cravens *et al.*, 1986) and model calculations (Strobel, 1971; Rees and Roble, 1979; Cravens *et al.*, 1979; Rusch and Sharp, 1981; Gérard *et al.*, 1984) have shown that the nitric oxide distribution depends in a complex way on latitude, local time, solar cycle, and magnetic activity. It is thus expected that the importance of the 5.3-μm cooling is also fairly variable in time and space. The geophysical conditions modeled in this study correspond to magnetically quiet periods at solar minimum solstice conditions for which the exospheric

temperature (global mean value = 820 K) and NO concentrations are relatively small ($\simeq 10^7$ cm^{-3} peak value near the equator). Even for these quiet conditions, NO radiative cooling perturbs the thermospheric dynamics and composition of the thermosphere. It is likely that the magnitude of this perturbation is larger during periods of higher u.v. solar flux and magnetic activity. Nitric oxide thermospheric concentrations depend on the magnitude of the ionospheric odd-nitrogen sources and N_2 dissociation rate which react to the modulation of the solar e.u.v. fluxes by the 11-year solar cycle (Garcia *et al.*, 1984). Magnetic storms generate temperature enhancements due to large Joule heating and increase the high-latitude production of NO by energetic particles. During these periods, large amounts of NO are present in the high-latitude thermosphere (Narcisi and Swider, 1976; Swider, 1978; Gérard *et al.*, 1983), and large 5.3-μm emission rates have been observed (Reidy *et al.*, 1982).

Acknowledgments—One of the authors (J-C.G.) is supported by the Belgian Foundation for Scientific Research (FNRS). This work was supported in part by NATO Cooperative Research Grant no 166/84 and by FRFC grant no. 2-4507-82. We acknowledge the National Center for Atmospheric Research for computing time. NCAR is sponsored by the National Science Foundation. We thank E. Deneye for his computational help.

REFERENCES

Bates, D. R. (1951) The temperature of the upper atmosphere. *Proc. Phys. Soc.* **64B**, 805.

Cravens, T. E. and Stewart, A. I. (1978) Global morphology of nitric oxide in the lower *E*-region. *J. geophys. Res.* **83**, 2446.

Cravens, T. E., Gérard, J. C., Stewart, A. I. and Rusch, D. W. (1979) The latitudinal gradient of nitric oxide in the lower thermosphere. *J. geophys. Res.* **84**, 2675.

Cravens, T. E., Gérard, J. C., Rusch, D. W., Stewart, A. I. and Lecompte, M. (1986) The global distribution of thermospheric nitric oxide as observed by the *Atmosphere Explorer D* satellite. *J. geophys. Res.* **90** (in press).

Dickinson, R. E. (1973) Method of parameterization for infrared cooling between altitudes of 30 and 70 kilometers. *J. geophys. Res.* **78**, 4451.

Dickinson, R. E., Ridley, E. C. and Roble, R. G. (1975) Meridional circulation in the thermosphere, I. Equinox conditions. *J. Atmos. Sci.* **32**, 1737.

Dickinson, R. E., Ridley, E. C. and Roble, R. G. (1977) Meridional circulation in the thermosphere, 2, solstice conditions. *J. Atmos. Sci.* **34**, 178.

Donahue, T. M. and Carignan, G. R. (1975) The temperature gradient between 100 and 120 km. *J. geophys. Res.* **80**, 4565.

Fernando, R. P. and Smith, I. W. M. (1979) Vibrational relaxation of NO by atomic oxygen. *Chem. Phys. Lett.* **66**, 218.

Garcia, R. R. and Solomon, S. (1983) A numerical model of the zonally-averaged dynamical and chemical structure of the middle atmosphere. *J. geophys. Res.* **88**, 1379.

Garcia, R. R., Solomon, S., Roble, R. G. and Rusch, D. W. (1948) A numerical response of the middle atmosphere to the 11-year solar cycle. *Planet. Space Sci.* **32**, 411.

Gérard, J-C. and Barth, C. A. (1977) High-latitude nitric oxide in the lower thermosphere. *J. geophys. Res.* **82**, 674.

Gérard, J-C., Deneye, E. J. and Singh, V. (1983) Rocket measurements and modelling of the nitric oxide distribution in the thermosphere and lower mesosphere. *Proceedings of the Sixth ESA symposium on European Rocket and Balloon Programmes* (*ESA SP*-183) 123.

Gérard, J. C., Roble, R. G., Rusch, D. W. and Stewart, A. I. (1984) The global distribution of thermospheric odd nitrogen for solstice conditions during solar cycle minimum. *J. geophys. Res.* **89**, 1725.

Gordiets, B. F. and Markov, M. N. (1977) Infrared radiation in the energy balance of the upper atmosphere. *Cosmic Res.* **15**, 633.

Gordiets, B. F., Markov, M. N. and Shelepin, L. A. (1978) I. R. radiation of the upper atmosphere. *Planet. Space Sci.* **26**, 933.

Gordiets, B. F., Kulirov, Y. N., Markov, M. N. and Marov, M. Y. (1982) Numerical modelling of the thermospheric heat budget. *J. geophys. Res.* **87**, 4504.

Grossman, K. U. and Offermann, D. (1978) Atomic oxygen emission at 63 μm as a cooling mechanism in the thermosphere and ionosphere. *Nature, Lond.* **276**, 594.

Heroux, L. and Higgins, J. E. (1977) Summary of full-dix solar fluxes between 250 and 1940 Å. *J. geophys. Res.* **82**, 3307.

Kockarts, G. (1975) Neutral atmosphere modeling, in *Atmospheres of the Earth and the Planets* (Edited by McCormac, B. M.), pp. 235–243. D. Reidel, Dordrecht.

Kockarts, G. (1980) Nitric oxide cooling in the terrestrial atmosphere. *Geophys. Res. Lett.* **7**, 137.

Kockarts, G. and Petermans, W. (1970) Atomic oxygen infrared emission in the earth's upper atmosphere. *Planet. Space Sci.* **18**, 271.

Kasting, J. F. and Roble, R. G. (1981) A zonally averaged chemical-dynamical model of the lower thermosphere. *J. geophys. Res.* **86**, 9641.

Lazarev, N. I. (1967) Absorption of the energy of an electron beam in the upper atmosphere. *Geomagn. Aeron.* **7**, 219.

Markov, M. N., Grechko, G. M., Gubarev, A. A., Ivanov, Y. S. and Petrov, V. S. (1977) Measurements of the nitric oxide infra-red spectrum in the midlatitude upper atmosphere for the orbiting space station Salyut 4. *Kosm. Issled.* **15**, 125.

Narcisi, R. C. and Swider, W. (1976) Ionic structure near an auroral arc. *J. geophys. Res.* **81**, 4770.

Ogawa, T. (1976) Excitation processes of infrared atmospheric emissions. *Planet. Space Sci.* **24**, 749.

Rawlins, W. T., Caledonia, G. E., Gibso, J. J. and Stair, A. T. (1981) Infrared emission from NO ($\Delta v = 1$) in an aurora: Spectral analysis and kinetic interpretation of HIRIS measurements. *J. geophys. Res.* **86**, 1313.

Rees, M. H. and Roble, R. G. (1979) The morphology of N and NO in auroral substorms. *Planet. Space Sci.* **27**, 453.

Reidy, W. P., Degges, T. C., Hurd, A. G., Stair, A. T. Jr. and Ulwick, J. C. (1982) Auroral nitric oxide concentration and infrared emission. *J. geophys. Res.* **87**, 3591.

Roble, R. G. and Emery, B. A. (1983) On the global mean temperature of the thermosphere. *Planet. Space Sci.* **31**, 597.

Roble, R. G. and Kasting, J. F. (1984) The zonally averaged circulation, temperature, and compositional structure of the lower thermosphere and variations with geomagnetic activity I. *J. geophys. Res.* **89**, 1711.

Roble, R. G., Dickinson, R. E. and Ridley, E. C. (1977) Seasonal and solar-cycle variations of the zonal mean circulation in the thermosphere. *J. geophys. Res.* **82**, 5493.

Rottman, G. J. (1981) Rocket measurements of the solar spectral irradiance during solar minimum, 1972–1977. *J. geophys. Res.* **86**, 6697.

Rusch, D. W. and Barth, C. A. (1975) Satellite measurements of nitric oxide in the polar region. *J. geophys. Res.* **80**, 3719.

Rusch, D. W. and Sharp, W. E. (1981) Nitric oxide delta band emission in the earth's atmosphere: Comparison of a measurement and a theory. *J. Geophys. Res.* **86**, 1011.

Solomon, S., Crutzen, P. J. and Roble, R. G. (1982) Photochemical coupling between the thermosphere and the lower atmosphere. *J. geophys. Res.* **87**, 7206.

Spiro, R. W., Reiff, P. F. and Maker, L. J. (1982) Precipitating electron energy flux and auroral zone conductances—An empirical model. *J. geophys. Res.* **87**, 8215.

Stair, A. T., Ulwick, J. C., Baker, K. D. and Baker, D. J. (1975) Rocket borne observations of atmospheric infrared emissions in the auroral region, in *Atmospheres of the Earth and the Planets* (Edited by McCormac, B. M.), p. 335. D. Reidel, Dordrecht.

Stewart, A. I. and Cravens, T. E. (1978) Diurnal and seasonal effects in E-region low-latitude nitric oxide. *J. geophys. Res.* **83**, 2453.

Strobel, D. F. (1971) Diurnal variation of nitric oxide in the upper atmosphere. *J. geophys. Res.* **76**, 2441.

Swider, W. (1978) Daytime nitric oxide at the base of the thermosphere. *J. geophys. Res.* **83**, 4407.

Torr, M. R., Torr, D. G., Ong, R. A. and Hinteregger, H. E. (1979) Ionization frequencies for major thermospheric constituents as a function of solar cycle 21. *Geophys. Res. Lett.* **6**, 771.

Torr, M. R., Torr, D. G. and Hinteregger, H. E. (1980) Solar flux variability in the Schumann-Runge continuum as a function of solar cycle 21. *J. geophys. Res.* **85**, 6063.